

---

# PixelVAE++: Improved PixelVAE with Discrete Prior

---

**Hossein Sadeghi**  
D-Wave Systems Inc.  
hsadeghi@dwavesys.com

**Evgeny Andriyash**  
D-Wave Systems Inc.  
eandriyash@dwavesys.com

**Walter Vinci**  
D-Wave Systems Inc.

**Lorenzo Buffoni**  
D-Wave Systems Inc.  
University of Florence  
lorenzo.buffoni@unifi.it

**Mohammad H. Amin**  
D-Wave Systems Inc.  
Simon Fraser University  
amin@dwavesys.com

## Abstract

Constructing powerful generative models for natural images is a challenging task. PixelCNN models capture details and local information in images very well but have limited receptive field. Variational autoencoders with a factorial decoder can capture global information easily, but they often fail to reconstruct details faithfully. PixelVAE combines the best features of the two models and constructs a generative model that is able to learn local and global structures. Here we introduce PixelVAE++, a VAE with three types of latent variables and a PixelCNN++ for the decoder. We introduce a novel architecture that reuses a part of the decoder as an encoder. We achieve the state of the art performance on binary data sets such as MNIST and Omniglot and achieve the state of the art performance on CIFAR-10 among latent variable models while keeping the latent variables informative.

## 1 Introduction

Generative modeling of images [1, 2, 3, 4, 5], audio [6, 7], and videos [8, 9] has advanced remarkably in the past few years and have resulted in great applications [10, 11]. Many machine learning tasks such as domain adaptation [12, 13, 14, 15] and few-shot learning [16, 17, 18] rely on learned representations of observations. The goal of generative learning is to model the distribution of unseen observations. This task is achieved with some degree of success by latent variable models such as variational autoencoder (VAE) [19, 20, 21, 4], flow-based models [22, 23, 24, 5], energy-based model [25], autoregressive models such as PixelCNN [26, 1, 27, 6, 28, 29], and lately, by the combination of latent-variable and autoregressive models, PixelVAE [30, 31].

While PixelCNN variants are able to model local correlations successfully, large models and self-attention mechanisms are necessary to capture long-range correlations [28]. VAEs, on the other hand, are able to capture global information in the latent space but generally fail to model local structure variations. Modelling the local structure, while not important for downstream tasks such as classification [32], is essential for building a powerful generative model. Early models with autoregressive decoder found that the autoregressive part learns all the features of the data and the latent variables are not used [33, 34, 35, 36, 37, 38]. Using a shallow PixelCNN decoder, PixelVAE [30] was able to achieve a generative performance comparable with PixelCNN, with hierarchical latent variables that meaningfully control the global features of generated images. However, in [31], authors argued that in principle the optimal point of a PixelVAE is where all information is modelled by the autoregressive part, but in practice this may not be achievable.

In this manuscript, we present PixelVAE++, a model that improves performance of PixelCNN++ and achieves state of the art performance on a few data sets. Our contribution can be summarized as follows:

- We combine PixelCNN++ architecture with VAEs. We show that using latent variables improves performance.
- We implement a hierarchical encoder that shares most of its parameters with the autoregressive decoder.
- We show that the choice of prior is essential in building a useful latent variable model. In particular, we use discrete latent variables with an RBM prior.

## 2 Background

PixelCNN [1] is an autoregressive generative model with a tractable likelihood. The model fully factorizes the probability density function as follow:

$$p(\mathbf{x}) = \prod_i p(x_i | \mathbf{x}_{<i}), \quad (1)$$

where  $\mathbf{x}_{<i}$  is the set of all  $x_j$  with  $j < i$ . The conditional distributions  $p(x_i | \mathbf{x}_{<i})$  are parameterized by convolutional neural networks. The functional forms of these conditionals are very flexible, making PixelCNN a powerful generative model. We used the most recent implementation of PixelCNN++ [26] that removes the blind spots and achieves better performance than previous PixelCNN models.

PixelVAE [30] is a VAE with PixelCNN as its decoder. Since its log-likelihood is intractable for large number of latent variables, the evidence lower bound (ELBO) is minimized as the objective function [19].

$$\mathcal{L}(\mathbf{x}) = \mathbb{E}_{\mathbf{z} \sim q(\mathbf{z}|\mathbf{x})} \left[ \log p_\theta(\mathbf{x}|\mathbf{z}) - \log \frac{p_\theta(\mathbf{z})}{q_\phi(\mathbf{z}|\mathbf{x})} \right] \leq \log p(\mathbf{x}) \quad (2)$$

where  $p_\theta(\mathbf{z})$  is the prior distribution over the latent variables  $\mathbf{z}$ , which together with conditional probability  $p_\theta(\mathbf{x}|\mathbf{z})$  forms the generative model  $p_\theta(\mathbf{x}, \mathbf{z})$  with parameters  $\theta$ , and  $q_\phi(\mathbf{z}|\mathbf{x})$  is the approximating posterior represented as a neural network with parameters  $\phi$ .

The conditional probability (decoder) and the approximating posterior (encoder) are trained end-to-end to optimize the generative and inference models jointly. Many researches around VAE models deal with building more expressive distributions for all its components [4, 39, 40, 30, 31]. PixelVAE in particular adds more power to the structure of the decoder by replacing conditionally independent dimensions with a fully autoregressive structure.

### 2.1 Discrete Variational Autoencoder (DVAE)

Restricted Boltzmann machines model multi-modal distributions and can capture complex relationship in data [41]. Using RBM as a prior in a generative model has been pioneered by [42] and later improved in [40, 43, 44, 45]. In order to back-propagate through the approximating posterior of discrete binary variables, we employ a continuous relaxation estimator that trades bias for variance [46, 47], in particular the Gumbel-Softmax estimator [48, 49]. Reference [45] showed that a relaxed (biased) objective can be used to train a DVAE with an RBM prior. The relaxed objective can be expressed as

$$\mathcal{L}(\mathbf{x}) = \mathbb{E}_{\rho \sim \mathbb{U}} \left[ \log p_\theta(\mathbf{x}|\boldsymbol{\zeta}_{\phi, \rho}) - \log \frac{p_\theta(\boldsymbol{\zeta}_{\phi, \rho})}{q_\phi(\boldsymbol{\zeta}_{\phi, \rho}|\mathbf{x})} \right] \quad (3)$$

where  $\rho$  is a random variable drawn from a uniform distribution  $\mathbb{U}$ , and  $\boldsymbol{\zeta}$  is the continuous relaxation of the discrete binary latent variables,

$$\boldsymbol{\zeta} = \sigma \left[ \frac{\mathbf{l}_\phi + \sigma^{-1}(\rho)}{\tau} \right] \quad (4)$$

with  $\sigma(x) = 1/(1 + e^{-x})$  being the sigmoid function,  $\mathbf{l}_\phi$  is the logit (output of a neural network), and  $\tau$  is the temperature that controls the sharpness of the function  $\boldsymbol{\zeta}$ . The continuous variable  $\boldsymbol{\zeta}$  is equal to the discrete variable  $\mathbf{z}$  in the limit  $\tau \rightarrow 0$ . At the test time only discrete variables are used which can be obtained by setting the temperature to zero.

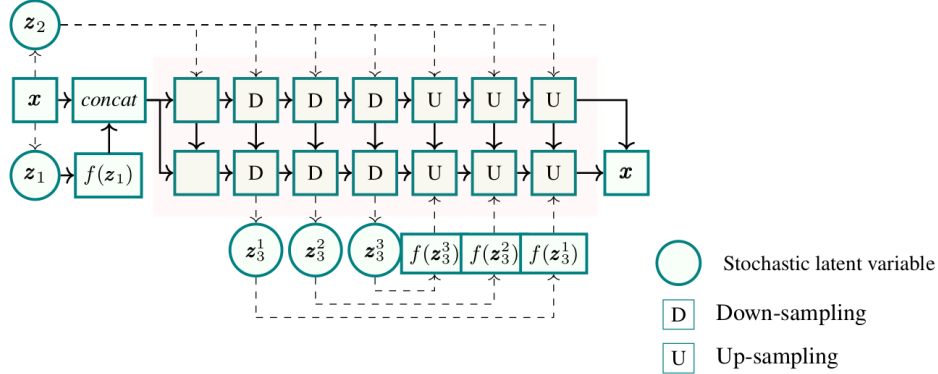
## 2.2 PixelVAE++ Architecture

For the decoder of the PixelVAE we implement a model similar to PixelCNN++ [26] using downward and rightward shifted image and feature maps. Similarly, we use 6 blocks of  $n$  ResNet layers, where  $n = 5$  for  $32 \times 32 \times 3$  inputs and smaller ( $n=3$ ) for  $28 \times 28$  inputs. Down sampling is performed between the 1st/2nd and 2nd/3rd blocks using convolutions with strides of 2, and up-sampling is performed between the 4th/5th and 5th/6th blocks. Similar to PixelCNN++, convolutional connections are introduced between early and late layers to ensure that details and fine structures are preserved at construction time.

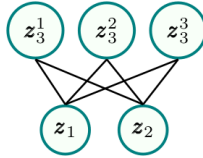
For the encoder, we use three groups of latent variables with a factorial Bernoulli distribution. The encoding distribution of the first group, *concatenated latent variables*  $z_1$ , is parameterized by convolutional neural networks (CNN) followed by a dense layer. Using deconvolutions with up-sampling, the decoder transforms the stochastic variables to the size of the input and then concatenates them with the input, similar to the original PixelVAE [30].

The parameters of the second encoding distribution is obtained by a separate set of CNN and dense layers. In the decoder, these *conditioning latent variables*  $z_2$  are added to activations before nonlinearities, similar to the conditional PixelCNN [1].

The architecture of the third group, the *shared latent variables*  $z_3$ , leverages the autoencoding structure of the PixelCNN++. There are  $(n + 1) \times 3$  layers up to the last down-sampling stage, where  $n$  ( $n = 5$  for CIFAR-10) is the number of ResNet layers per block. Each layer  $h_{b,i}$  ( $b$ -block index,  $i$ -ResNet layer index) with the size  $[B, H, W, N]$ , ([batch size, height, width, filters]) is reduced to a  $[B, 8, 8, 1]$  by convolution and is followed by a dense layer to 64 variables to produce the logits of the Bernoulli distribution. Each latent variable is then transformed by a dense layer, followed by up-sampling to the same size as  $h_{b,i}$ . The transformed stochastic variable is concatenated with  $h_{b,i}$  and is passed to the corresponding up-sampling block  $h_{7-b,n+1-i}$ . A gated ResNet combines this layer and the transformed latent variables. A schematic drawing is presented in Fig. 1.



(a) PixelVAE++ architecture



(b) RBM Prior

Figure 1: The hierarchical structure of PixelVAE++ with RBM prior. Arrows indicate convolutional connection with autoregressive structure. Dashed arrows indicate convolutional connection. The decoder and encoder structures are fused together. The series of down-sampling stages that constitute a of the decoder for  $z_1$  and  $z_2$  variables, acts as an encoder for  $z_3$  variables. Note that the skip connections in the decoder part is omitted in the model graph to reduce clutter.

### 3 Experiments

We study the performance of PixelVAE++ for density estimation on 2D images. The experiments are performed on statically and dynamically [50] binarized MNIST, Omniglot, and Caltech-101 silhouettes [51] and CIFAR-10 [52]. For all data sets, we use the standard allocation of training, validation, and test sets. We trained the models for 500 epochs on one GPU for binary data sets and 1000 epochs on 8 GPUS for CIFAR-10. Our goal is to determine whether we can improve the performance of PixelCNN++ with VAE and to understand what effect the use of discrete binary latent variables has on the performance of PixelVAE++, if any.

#### 3.1 Performance of PixelVAE++

Some inputs have  $28 \times 28$  binary pixel images. We use the same architecture for the MNIST and Omniglot data sets with 3 ResNet layers per block, each having 64 feature maps. Because the Caltech-101 silhouettes data set is smaller, our model with PixelCNN++ decoder using strides of 2 for down-sampling and up-sampling, easily over-fits. We remove the strides and reduce the number of feature maps to 32, but keep the number of ResNet layers the same. We found that for input sizes of  $28 \times 28$ , only three ResNet layers per block was needed to achieve optimal performance. The Log-Likelihood (LL) is evaluated using 1000 importance weighted samples [53]. We were able to achieve better performance than what is already published on dynamically binarized MNIST using PixelCNN++ and we further improve the LL using PixelVAE++. The LL reaches the values of -78.00 and -88.29 for MNIST (Dynamic) and Omniglot, respectively. We obtained this results by including only the first group of latent variables, but we also experimented with including all three categories of latent variables. Only the first category, the concatenated variables, was necessary and sufficient for optimal LL in these data sets and adding the other groups did not improve results. We have repeated the experiments for each data set three times and have reported the average. The standard deviation for the mean is  $\pm 0.04$ , therefore the last digit is uncertain. However, we have followed the norm to report the results for the binary data sets up to the second digit.

For the binary data sets, we use 400 binary variables in the latent space all of which belong to concatenated latent variables. The prior consists of an RBM with 200 variables on each side of the bipartite graph. We sample from the RBM during training to computing the gradients of the log-partition function. We use 5000 samples obtained by annealed importance sampling (AIS) [54] with 1000 temperatures steps and 50 MCMC update per step. For the evaluation of the log-partition function, we increase the number of samples and temperature steps tenfold. For training we used batch sizes of 128 samples.

Experiments on CIFAR-10 are done using the same set of hyper-parameters and network architecture as in PixelCNN++ [26], except for the number of filters which we reduce from 160 to 128. We use batch sizes of 8 samples per GPU or 64 samples in total. We only add and tune VAE related parameters and hyper-parameters. Our model has 40 M parameters, including 6 M for VAE, as compared to 54 M in the original PixelCNN++. Despite the reduced number of parameters, the negative log-likelihood in bpd reaches 2.90. The decoder alone with 128 filters only reaches 2.95 bpd, higher than 2.92 bpd with 160 filters. Increasing the number of filters back to 160 for the VAE model did not result in a better performance than 2.90 bpd. The details of the implementation is outlined in the appendix A for  $32 \times 32 \times 3$  inputs. The numbers are reported after averaging three independent runs with a standard deviation of  $\pm 0.001$ . The standard deviation of log-likelihood for different evaluations of importance weighted sum is negligible.

For the CIFAR-10 data set, we use an architecture that includes all three groups of latent variables: 512 concatenated, 128 conditional, and  $8 \times 8 \times 3 \times (n+1)$  shared. To construct the RBM, we place the first two groups on one side and the shared variables on the other side of the fully visible RBM. Due to the increased size of the RBM and to reduce the computational cost of AIS we use only 500 samples for training and 5000 samples for evaluation.

#### 3.2 Conditional image generation

We perform experiments with PixelVAE++ to assess generation of images conditional on the latent variables given by the approximating posterior. We generate samples using the latent variables inferred from test images. Figures 2 and 3 show reconstructed images from MNIST and Omniglot

MNIST	Static		Dynamic	
	LL	KL	LL	KL
PixelVAE++ Gaussian	-78.66	6.86	-78.01	4.2
PixelVAE++ RBM	<b>-78.65</b>	7.62	<b>-78.00</b>	5.05
VLAE	-79.03		-78.53	

	OMNIGLOT		Caltech 101	
	LL	KL	LL	KL
PixelVAE++ Gaussian	-88.65	1.63	-79.52	4.00
PixelVAE++ RBM	<b>-88.29</b>	2.56	-77.46	6.85
VLAE	-89.83		<b>-77.36</b>	

bpd	CIFAR10	
	LL	KL
PixelVAE++ Gaussian	2.92	0.005
PixelVAE++ RBM	2.90	0.016
VLAE	2.95	
PixelCNN++	2.92	
PixelSNAIL	<b>2.85</b>	

Table 1: This table summarizes the results for PixelVAE++ experiments on multiple data sets.

test sets for PixelVAE++ trained with RBM and Gaussian priors. As evident from Fig. 2, both models with continuous and discrete priors construct the digits very well. Despite having similar LL, the model with the RBM prior has a sharp conditional distribution that captures small variations in digit shape, while the one with the Gaussian prior has much broader conditional, that can cover multiple digit classes. For Omniglot data set (Fig. 3), the model with RBM prior similarly has a sharper conditional, although in this case both RBM and Gaussian prior models span multiple object classes.

The similarity of the reconstructed image and the original one can be measured equivalently by conditional probability, KL divergence of approximating posterior from prior (for a fixed ELBO), and the mutual information between  $\mathbf{x}$  and  $\mathbf{z}$ , all of which change monotonically with respect to each other [55]. We report the KL divergence in table 1. It is evident from the images and the KL values that PixelVAE++ with RBM prior is able to learn models with sharper decoder distributions and more informative latent space than the one with Gaussian prior.

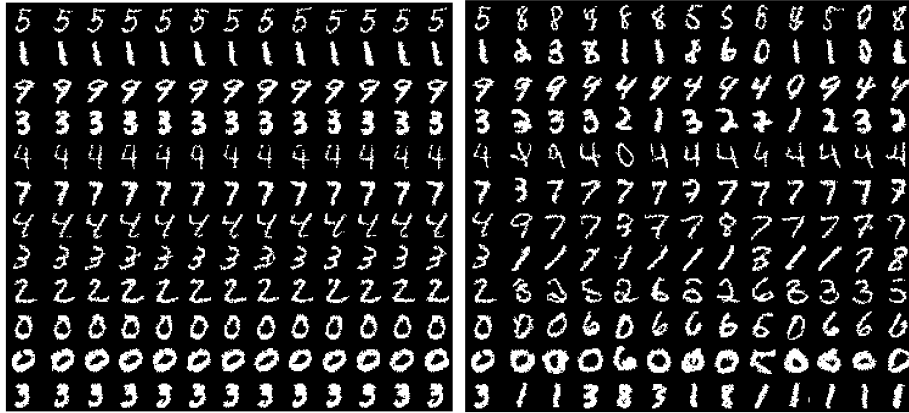


Figure 2: Reconstructed samples for a PixelVAE++ trained on MNIST. Each row is generated from latent variables inferred from the image in the first column. The prior distributions are RBM (left) and Gaussian (right).

For the case of CIFAR-10 images, the decoder distribution becomes rather broad as illustrated in figure 4. To visually highlight how this distribution varies over the data set we choose 128 data points, sample 8 images conditioned on the latent representation of each data point, and then display the ones with the smallest mutual energy distance [26] on the left panel, and largest on the right. It is hardly possible to categorize images conditioned on the same latent variable as belonging to the same

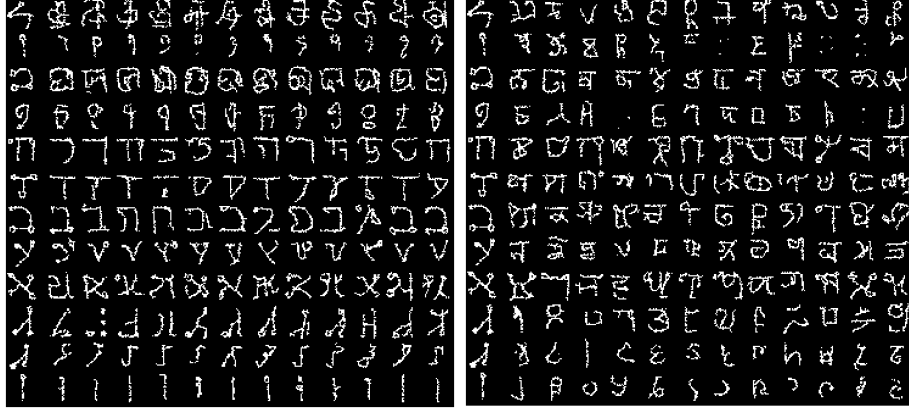


Figure 3: Reconstructed samples for a PixelVAE++ trained on Omniglot. Each row is generated from latent variables inferred from the image in the first column. The prior distributions are RBM (left) and Gaussian (right).

class, but in some cases it is possible to argue that images are similar in some global appearances such as color and composition.



Figure 4: Reconstructed samples for a PixelVAE++ trained on CIFAR-10. Each row is generated from latent variables inferred from the images in the first column. The prior distribution used for training is an RBM. We have sorted rows based on energy distance from the test images and put the first 8 with the closest distance on the left panel and the last 8 on the right panel.

## 4 Conclusions

We have presented a VAE model using an autoregressive decoder that performs well in generative tasks, in terms of LL, and makes use of the latent variables. This model achieves the best performance among other latent variable models on CIFAR-10 data set by reaching LL of 2.90 bpd using 25% less parameters than PixelCNN++.

For the binary data sets, the discrete latent variables capture global features of images (like digit class) while the decoder distribution models local variations.

For more complex natural images, the latent variables help autoregressive model to represent some global features, like color and composition, and achieve better performance in terms of log-likelihood.

## References

- [1] Aaron Van den Oord, Nal Kalchbrenner, Lasse Espeholt, Oriol Vinyals, Alex Graves, et al. Conditional image generation with pixelcnn decoders. In *Advances in Neural Information Processing Systems*, pages 4790–4798, 2016.
- [2] Ian J. Goodfellow, Jean Pouget-Abadie, Mehdi Mirza, Bing Xu, David Warde-Farley, Sherjil Ozair, Aaron Courville, and Yoshua Bengio. Generative Adversarial Networks. *arXiv:1406.2661 [cs, stat]*, June 2014. arXiv: 1406.2661.
- [3] Karol Gregor, Frederic Besse, Danilo Jimenez Rezende, Ivo Danihelka, and Daan Wierstra. Towards conceptual compression. In *Advances In Neural Information Processing Systems*, pages 3549–3557, 2016.
- [4] Durk P Kingma, Tim Salimans, Rafal Jozefowicz, Xi Chen, Ilya Sutskever, and Max Welling. Improved variational inference with inverse autoregressive flow. In *Advances in neural information processing systems*, pages 4743–4751, 2016.
- [5] Laurent Dinh, Jascha Sohl-Dickstein, and Samy Bengio. Density estimation using real nvp. *arXiv preprint arXiv:1605.08803*, 2016.
- [6] Aaron van den Oord, Sander Dieleman, Heiga Zen, Karen Simonyan, Oriol Vinyals, Alex Graves, Nal Kalchbrenner, Andrew Senior, and Koray Kavukcuoglu. Wavenet: A generative model for raw audio. *arXiv preprint arXiv:1609.03499*, 2016.
- [7] Soroush Mehri, Kundan Kumar, Ishaan Gulrajani, Rithesh Kumar, Shubham Jain, Jose Sotelo, Aaron Courville, and Yoshua Bengio. Samplernn: An unconditional end-to-end neural audio generation model. *arXiv preprint arXiv:1612.07837*, 2016.
- [8] Nal Kalchbrenner, Aäron van den Oord, Karen Simonyan, Ivo Danihelka, Oriol Vinyals, Alex Graves, and Koray Kavukcuoglu. Video pixel networks. In *Proceedings of the 34th International Conference on Machine Learning-Volume 70*, pages 1771–1779. JMLR. org, 2017.
- [9] Chelsea Finn, Ian Goodfellow, and Sergey Levine. Unsupervised learning for physical interaction through video prediction. In *Advances in neural information processing systems*, pages 64–72, 2016.
- [10] Christian Ledig, Lucas Theis, Ferenc Huszár, Jose Caballero, Andrew Cunningham, Alejandro Acosta, Andrew Aitken, Alykhan Tejani, Johannes Totz, Zehan Wang, et al. Photo-realistic single image super-resolution using a generative adversarial network. In *Proceedings of the IEEE conference on computer vision and pattern recognition*, pages 4681–4690, 2017.
- [11] Phillip Isola, Jun-Yan Zhu, Tinghui Zhou, and Alexei A Efros. Image-to-image translation with conditional adversarial networks. In *Proceedings of the IEEE conference on computer vision and pattern recognition*, pages 1125–1134, 2017.
- [12] Judy Hoffman, Erik Rodner, Jeff Donahue, Trevor Darrell, and Kate Saenko. Efficient learning of domain-invariant image representations. *arXiv preprint arXiv:1301.3224*, 2013.
- [13] Muhammad Ghifary, W Bastiaan Kleijn, and Mengjie Zhang. Domain adaptive neural networks for object recognition. In *Pacific Rim international conference on artificial intelligence*, pages 898–904. Springer, 2014.
- [14] Konstantinos Bousmalis, Nathan Silberman, David Dohan, Dumitru Erhan, and Dilip Krishnan. Unsupervised pixel-level domain adaptation with generative adversarial networks. In *Proceedings of the IEEE conference on computer vision and pattern recognition*, pages 3722–3731, 2017.
- [15] Mei Wang and Weihong Deng. Deep visual domain adaptation: A survey. *Neurocomputing*, 312:135–153, 2018.
- [16] Sachin Ravi and Hugo Larochelle. Optimization as a model for few-shot learning. 2016.
- [17] Adam Santoro, Sergey Bartunov, Matthew Botvinick, Daan Wierstra, and Timothy Lillicrap. One-shot learning with memory-augmented neural networks. *arXiv preprint arXiv:1605.06065*, 2016.
- [18] Jake Snell, Kevin Swersky, and Richard Zemel. Prototypical networks for few-shot learning. In *Advances in Neural Information Processing Systems*, pages 4077–4087, 2017.

- [19] Diederik P Kingma and Max Welling. Auto-encoding variational bayes. *arXiv preprint arXiv:1312.6114*, 2013.
- [20] Danilo Jimenez Rezende, Shakir Mohamed, and Daan Wierstra. Stochastic backpropagation and approximate inference in deep generative models. *arXiv preprint arXiv:1401.4082*, 2014.
- [21] Tim Salimans, Diederik P Kingma, Max Welling, et al. Markov chain monte carlo and variational inference: Bridging the gap. In *ICML*, volume 37, pages 1218–1226, 2015.
- [22] Durk P Kingma and Prafulla Dhariwal. Glow: Generative flow with invertible 1x1 convolutions. In *Advances in Neural Information Processing Systems*, pages 10236–10245, 2018.
- [23] Danilo Jimenez Rezende and Shakir Mohamed. Variational inference with normalizing flows. *arXiv preprint arXiv:1505.05770*, 2015.
- [24] Laurent Dinh, David Krueger, and Yoshua Bengio. Nice: Non-linear independent components estimation. *arXiv preprint arXiv:1410.8516*, 2014.
- [25] Yilun Du and Igor Mordatch. Implicit generation and generalization in energy-based models. *arXiv preprint arXiv:1903.08689*, 2019.
- [26] Tim Salimans, Andrej Karpathy, Xi Chen, and Diederik P Kingma. PixelCNN++: Improving the pixelCNN with discretized logistic mixture likelihood and other modifications. *arXiv preprint arXiv:1701.05517*, 2017.
- [27] Aäron Van Den Oord, Nal Kalchbrenner, and Koray Kavukcuoglu. Pixel recurrent neural networks. In *Proceedings of the 33rd International Conference on International Conference on Machine Learning*, pages 1747–1756. JMLR. org, 2016.
- [28] Xi Chen, Nikhil Mishra, Mostafa Rohaninejad, and Pieter Abbeel. Pixelsnail: An improved autoregressive generative model. *arXiv preprint arXiv:1712.09763*, 2017.
- [29] Mathieu Germain, Karol Gregor, Iain Murray, and Hugo Larochelle. Made: Masked autoencoder for distribution estimation. In *International Conference on Machine Learning*, pages 881–889, 2015.
- [30] Ishaan Gulrajani, Kundan Kumar, Faruk Ahmed, Adrien Ali Taiga, Francesco Visin, David Vazquez, and Aaron Courville. Pixelvae: A latent variable model for natural images. *arXiv preprint arXiv:1611.05013*, 2016.
- [31] Xi Chen, Diederik P Kingma, Tim Salimans, Yan Duan, Prafulla Dhariwal, John Schulman, Ilya Sutskever, and Pieter Abbeel. Variational lossy autoencoder. *arXiv preprint arXiv:1611.02731*, 2016.
- [32] Yoshua Bengio. Deep learning of representations: Looking forward. In *International Conference on Statistical Language and Speech Processing*, pages 1–37. Springer, 2013.
- [33] Otto Fabius and Joost R van Amersfoort. Variational recurrent auto-encoders. *arXiv preprint arXiv:1412.6581*, 2014.
- [34] Samuel R Bowman, Luke Vilnis, Oriol Vinyals, Andrew M Dai, Rafal Jozefowicz, and Samy Bengio. Generating sentences from a continuous space. *arXiv preprint arXiv:1511.06349*, 2015.
- [35] Junyoung Chung, Caglar Gulcehre, KyungHyun Cho, and Yoshua Bengio. Empirical evaluation of gated recurrent neural networks on sequence modeling. *arXiv preprint arXiv:1412.3555*, 2014.
- [36] Iulian V Serban, Alessandro Sordoni, Yoshua Bengio, Aaron Courville, and Joelle Pineau. Building end-to-end dialogue systems using generative hierarchical neural network models. In *Thirtieth AAAI Conference on Artificial Intelligence*, 2016.
- [37] Iulian Vlad Serban, Alessandro Sordoni, Ryan Lowe, Laurent Charlin, Joelle Pineau, Aaron Courville, and Yoshua Bengio. A hierarchical latent variable encoder-decoder model for generating dialogues. In *Thirty-First AAAI Conference on Artificial Intelligence*, 2017.
- [38] Marco Fraccaro, Søren Kaae Sønderby, Ulrich Paquet, and Ole Winther. Sequential neural models with stochastic layers. In *Advances in neural information processing systems*, pages 2199–2207, 2016.
- [39] Jakub M Tomczak and Max Welling. Vae with a vampprior. *arXiv preprint arXiv:1705.07120*, 2017.



- [40] Arash Vahdat, William G Macready, Zhengbing Bian, Amir Khoshaman, and Evgeny Andriyash. Dvae++: Discrete variational autoencoders with overlapping transformations. *arXiv preprint arXiv:1802.04920*, 2018.
- [41] Nicolas Le Roux and Yoshua Bengio. Representational power of restricted boltzmann machines and deep belief networks. *Neural computation*, 20(6):1631–1649, 2008.
- [42] Jason Tyler Rolfe. Discrete variational autoencoders. *arXiv preprint arXiv:1609.02200*, 2016.
- [43] Arash Vahdat, Evgeny Andriyash, and William G Macready. DVAE#: Discrete variational autoencoders with relaxed Boltzmann priors. In *Neural Information Processing Systems (NIPS)*, 2018.
- [44] Arash Vahdat, Evgeny Andriyash, and William G Macready. Learning undirected posteriors by backpropagation through mcmc updates. *arXiv preprint arXiv:1901.03440*, 2019.
- [45] Amir H Khoshaman and Mohammad Amin. Gumbolt: Extending gumbel trick to boltzmann priors. In *Advances in Neural Information Processing Systems*, pages 4065–4074, 2018.
- [46] Yoshua Bengio, Nicholas Léonard, and Aaron Courville. Estimating or propagating gradients through stochastic neurons for conditional computation. *arXiv preprint arXiv:1308.3432*, 2013.
- [47] Tapani Raiko, Mathias Berglund, Guillaume Alain, and Laurent Dinh. Techniques for learning binary stochastic feedforward neural networks. *arXiv preprint arXiv:1406.2989*, 2014.
- [48] Eric Jang, Shixiang Gu, and Ben Poole. Categorical reparameterization with gumbel-softmax. *arXiv preprint arXiv:1611.01144*, 2016.
- [49] Chris J Maddison, Andriy Mnih, and Yee Whye Teh. The concrete distribution: A continuous relaxation of discrete random variables. *arXiv preprint arXiv:1611.00712*, 2016.
- [50] Yann LeCun, Léon Bottou, Yoshua Bengio, and Patrick Haffner. Gradient-based learning applied to document recognition. *Proceedings of the IEEE*, 86(11):2278–2324, 1998.
- [51] Benjamin Marlin, Kevin Swersky, Bo Chen, and Nando Freitas. Inductive principles for restricted Boltzmann machine learning. In *Proceedings of the Thirteenth International Conference on Artificial Intelligence and Statistics*, pages 509–516, 2010.
- [52] Alex Krizhevsky and Geoffrey Hinton. Learning multiple layers of features from tiny images. Technical report, Citeseer, 2009.
- [53] Yuri Burda, Roger Grosse, and Ruslan Salakhutdinov. Importance weighted autoencoders. *arXiv preprint arXiv:1509.00519*, 2015.
- [54] Radford M Neal. Annealed importance sampling. *Statistics and computing*, 11(2):125–139, 2001.
- [55] Alexander A Alemi, Ben Poole, Ian Fischer, Joshua V Dillon, Rif A Saurous, and Kevin Murphy. Fixing a broken elbo. *arXiv preprint arXiv:1711.00464*, 2017.
- [56] Sergey Ioffe and Christian Szegedy. Batch normalization: Accelerating deep network training by reducing internal covariate shift. In *International Conference on Machine Learning*, pages 448–456, 2015.
- [57] Nitish Srivastava, Geoffrey Hinton, Alex Krizhevsky, Ilya Sutskever, and Ruslan Salakhutdinov. Dropout: a simple way to prevent neural networks from overfitting. *The Journal of Machine Learning Research*, 15(1):1929–1958, 2014.
- [58] Tim Salimans and Durk P Kingma. Weight normalization: A simple reparameterization to accelerate training of deep neural networks. In *Advances in Neural Information Processing Systems*, pages 901–909, 2016.
- [59] Casper Kaae Sønderby, Tapani Raiko, Lars Maaløe, Søren Kaae Sønderby, and Ole Winther. Ladder variational autoencoders. In *Advances in neural information processing systems*, pages 3738–3746, 2016.
- [60] Geoffrey Roeder, Yuhuai Wu, and David K Duvenaud. Sticking the landing: Simple, lower-variance gradient estimators for variational inference. In *Advances in Neural Information Processing Systems*, pages 6925–6934, 2017.

## A Network architecture details

The table 2 outlines the details of the implementation for the CIFAR-10 experiment.

Module	Type	CIFAR-10
$q(\mathbf{z}_1 \mathbf{x})$	convolutional + dense	64↓, 64, 64↓, 64, 64↓, 64, 64↓, 64, 512 FC
$f(\mathbf{z}_1)$	dense + deconvolutional	512 FC, 64↑, 64, 64↑, 64, 64↑, 64, 16↑, 16, 3↑
$q(\mathbf{z}_2 \mathbf{x})$	convolutional + dense	1↓, 128 FC
$q(\mathbf{z}_3^1 \mathbf{h}_3^1(\mathbf{x}))$	convolutional + dense	1↓(Kernel = Stride = 4), 64 FC
$q(\mathbf{z}_3^2 \mathbf{h}_3^2(\mathbf{x}))$	convolutional + dense	1↓, 64 FC
$q(\mathbf{z}_3^3 \mathbf{h}_3^3(\mathbf{x}))$	convolutional + dense	1, 64 FC
$f(\mathbf{z}_3^1)$	dense + deconvolutional	64 FC, 128↑(Kernel = Stride = 4)
$f(\mathbf{z}_3^2)$	dense + deconvolutional	64 FC, 128↑
$f(\mathbf{z}_3^3)$	dense + deconvolutional	64 FC, 128

Table 2: The details of the implementation. The functions with  $q$  are encoding distributions parameterized by neural networks while functions with  $f$  are deterministic transformation of latent variables. The arrow signs pointing up and down indicate up-sampling and down-sampling stages in the network. The symbols  $h_i^j$  denote the deterministic hidden variables for the latent variables of group  $i$  and subgroup  $j$ .

## B Improving optimization

Techniques such as batch normalization [56], dropout [57], weight normalization [58], and learning-rate decay can significantly improve the performance of a PixelVAE. We evaluate PixelVAE++ by comparing the training of the model to the original PixelCNN++ , both of which include these improvements. For a fair comparison, we apply only those techniques that were also used in [26]. We examine whether adding a VAE structure to the PixelCNN++ would improve the performance.

For VAE specifically, we use optimization methods such as KL annealing [59] which is shown to prevent the approximating posterior from falling into a local minimum.

When we use RBM as the prior, the KL term of the VAE doesn't have a closed form. We reduce the variance of the optimization by neglecting the derivatives of the form  $\partial_\phi q_\phi(\mathbf{z}|\mathbf{x})$  and instead the encoder is only trained by the path derivatives [60].

## C Temperature annealing

The temperature  $\tau$  for continuous relaxation (3) determines the trade-off between bias and variance. While low temperature relaxation is less biased, its derivative has high variance. We find that a temperature around 0.25 is sufficient to achieve best performance for all experiments. If the temperature is too high (0.5), the mismatch between the smoothed posterior and the RBM grows rapidly. If the temperature is too low (0.1) the high variance of the gradient prevents convergence to below 2.98 bpd in CIFAR-10 experiment.

We experimented with annealing the temperature from high to low and vice versa. The intuition for annealing to high temperature is to reduce variance towards the end of the optimization, and lowering temperature aims at reducing the bias towards the end while keeping the beginning of the training high variance in order to help keeping away from a local minima. In practice however, we find decreasing temperature to degrade performance and increasing it to have no effect compared to training with the final temperature all the way through. This is perhaps due to the high variance of training VAEs and therefore adding the variance due to low temperature has no meaningful effect.

## D Image generation

We evaluate the generated samples conditional on the prior distribution. To sample from the RBM prior, we perform 50000 Gibbs block sampling updates. While the cost of these updates for 1792

variables may be too much for the training phase, it is negligible compared to the autoregressive generation with deep neural networks of 40M variables. With a fixed RBM samples, we then generate multiple samples from the decoder.

For MNIST and Omniglot, the generated samples are fairly sharp (Fig. 5 and Fig. 6). As show in figure 5, samples from the model with RBM prior are generally fall in the same mode but occasionally change, however, the same change occurs more frequently when the prior is Gaussian.

For CIFAR-10, there is hardly any similarity between the images. To visualize the similarity of the images (if any), we generated 128 RBM samples and 8 images per sample in each row and then sorted the rows based on the mutual energy distance [26]. We put the first 8 rows with the smallest mutual energy distance in the left panel and the last 8 rows on the right panel of figure 7. We also experimented with other metrics such as mutual  $L_1$  and  $L_2$  distances. In all cases there is hardly any similarity between the generated samples as in figure 7. While discrete latent variables capture the structure of the data well in smaller data sets (MNIST, Omniglot), neither the discrete nor continuous variables capture the structure in the CIFAR-10 data set.

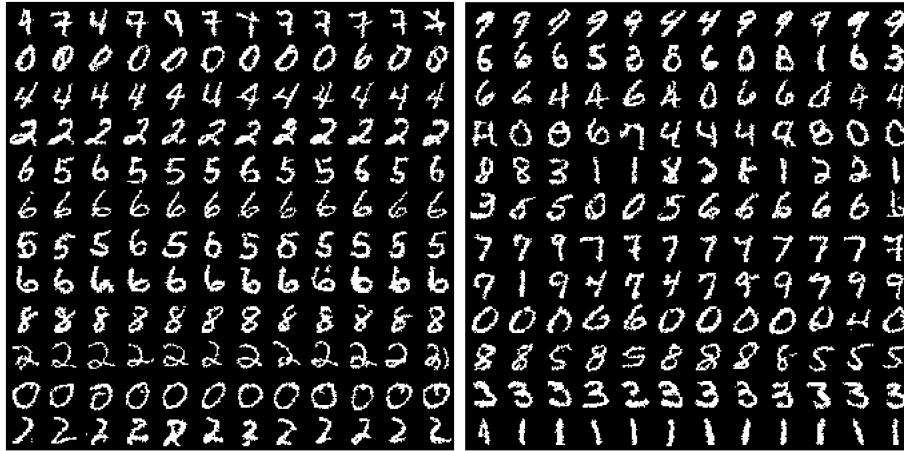


Figure 5: Generated samples for a PixelVAE++ trained on MNIST. Each row is generated from latent variables sampled from the prior distribution. The prior distributions are RBM (left) and Gaussian (right).



Figure 6: Generated samples for a PixelVAE++ trained on Omniglot. Each row is generated from latent variables sampled from the prior distribution. The prior distributions are RBM (left) and Gaussian (right).



Figure 7: Generated samples. Each row corresponds to the same latent variable. Out of 128 row, we picked 8 with the smallest (left) and largest (right) mutual energy distance [26].